Ecotoxicology and Environmental Safety 309 (2026) 119677

Contents lists available at ScienceDirect

Ecotoxicology and Environmental Safety

journal homepage: www.elsevier.com/locate/ecoenv

Integrated analysis of detoxification pathways and hepatotoxicity of butylated hydroxytoluene (BHT) in the Manila clam (*Ruditapes philippinarum*)

Ruicheng Qi [a], Pengfei Li [a], Qiaoqiao Wang [a], Jingjing Miao [a], Zeyuan Li [a,b,*], Luqing Pan [a,**]

[a] Key Laboratory of Mariculture, Ministry of Education, Ocean University of China, Qingdao 266003, PR China
[b] Aquatic Ecology and Water Quality Management Group, Wageningen University & Research, Wageningen, the Netherlands

ARTICLE INFO

Edited by Dr Hyo-Bang Moon

Keywords:
Synthetic phenolic antioxidants
Butylated hydroxytoluene
Ruditapes philippinarum
Detoxification pathway
Hepatotoxicity

ABSTRACT

Synthetic phenolic antioxidants (SPAs) are emerging contaminants (ECs) of growing concern in marine ecosystems, yet their detoxification and hepatotoxicity in marine invertebrates remain largely unknown. Here, we integrated transcriptomic profiling, in *silico* prediction, and experimental validation to characterize the detoxification of butylated hydroxytoluene (BHT) in *Ruditapes philippinarum* and to elucidate its hepatotoxicity. BHT metabolism was transcriptionally regulated by the aryl hydrocarbon receptor (*AHR*) and hormone receptor 96 (*HR96*) pathways. Key enzymes included Phase I cytochrome P450 isoforms (*CYP1A1, CYP1A2, CYP3A4*) and the Phase II enzyme UDP-glucuronosyltransferase (*UGT*). Metabolite profiling revealed the transformation products in the order: BHT-CHO > BHT-Q > BHT-OH > BHT-COOH, and a cascade detoxification pathway was subsequently proposed. BHT exposure impaired antioxidant defenses, induced oxidative stress, and caused macromolecular damage. Molecular dynamics simulations revealed a compromised DPPC bilayer integrity, suggesting structural membrane damage. In parallel, histopathological analysis exhibited characteristic hepatic lesions and cytoplasmic vacuolization, accompanied by significant increases in inflammatory cytokines (*TNF*, *IL16*) and transaminase levels (AST, ALT). Together, these results delineate a metabolism–oxidative stress–hepatotoxicity cascade for BHT in bivalves, providing novel mechanistic insights into SPA-induced toxicity. Our findings highlight the ecological risks posed by persistent SPAs in marine environments and underscore their potential to compromise the health of sentinel bivalves, supporting their inclusion in environmental monitoring and regulatory frameworks.

1. Introduction

Over the past decades, the rapid expansion in chemical production and use has led to the widespread release of numerous compounds into the environment without comprehensive risk assessment (Johnson et al., 2020; Ruan et al., 2023). Among these, synthetic phenolic antioxidants (SPAs) have emerged as a class of emerging contaminants (ECs) of increasing concern due to their extensive application in food, pharmaceuticals, plastics, and rubber products, as well as their frequent detection in aquatic environments, including surface waters, sediments, and bivalve mollusks (Liu and Mabury, 2020; ReportLinker, 2023; Wang et al., 2024). Accumulating evidence indicates that SPAs exhibit diverse toxicological effects, such as neurotoxicity, endocrine disruption, immunotoxicity, reproductive toxicity, and developmental toxicity, highlighting their potential ecological risks in aquatic ecosystems (Alofe et al., 2019; Liu et al., 2022; Chai et al., 2023; Yang et al., 2023; Li et al., 2024). However, the metabolic fate and detoxification mechanisms of SPAs in aquatic organisms remain insufficiently understood, particularly in invertebrates (Zhang et al., 2022).

The toxicological outcomes of environmental contaminants are largely determined by their metabolic transformation within organisms. Xenobiotics typically undergo a multistage biotransformation process involving Phase 0 efflux transporters, Phase I metabolic activation mediated primarily by cytochrome P450 (CYP450) enzymes, Phase II conjugation, and Phase III excretion via ATP-binding cassette transporters (Ashrap et al., 2017; Dong et al., 2024). Notably, metabolic

* Corresponding author at: Aquatic Ecology and Water Quality Management Group, Wageningen University & Research, Wageningen, the Netherlands.
** Correspondence to: Fisheries College, Ocean University of China, Yushan Road 5, Qingdao, Qingdao 266003, PR China.
E-mail addresses: zeyuan.li@wur.nl (Z. Li), panlq@ouc.edu.cn (L. Pan).

https://doi.org/10.1016/j.ecoenv.2026.119677
Received 26 August 2025; Received in revised form 30 December 2025; Accepted 1 January 2026
Available online 5 January 2026

activation by Phase I enzymes is a critical step that can enhance the toxicity of many organic pollutants (Tian et al., 2023). While the metabolism and regulatory pathways of SPAs have been partially characterized in vertebrates, their detoxification processes and the roles of xenobiotic nuclear receptors in aquatic invertebrates remain poorly elucidated (Holaas et al., 2008; Zhang et al., 2020; Li et al., 2025a). In this context, in *silico* approaches, including metabolic prediction and molecular docking, have become valuable tools for identifying potential metabolic pathways and key molecular targets, especially when integrated with experimental validation (Chibwe et al., 2017; Xie et al., 2023; Zhang et al., 2024a).

In vertebrates, the liver is the central organ responsible for xenobiotic metabolism and detoxification, and pollutant-induced liver injury is commonly associated with oxidative stress, inflammation, apoptosis, and metabolic disorders (Wang et al., 2023; Zhang et al., 2025; Li et al., 2025b). Although aquatic invertebrates lack a morphologically defined liver, the digestive gland of bivalves serves a functionally analogous role, integrating digestion, metabolism, and detoxification (Petushok et al., 2002; Rodrigo and Costa, 2017; Lobo-da-Cunha, 2019). Despite its ecological relevance, hepatotoxicity in aquatic invertebrates has received limited attention, and mechanistic frameworks and reliable biomarkers for assessing digestive gland injury under organic pollutant stress remain underdeveloped (Li et al., 2023; Zhang et al., 2024b). Previous studies have shown that SPAs can induce oxidative stress and tissue damage in the digestive glands of bivalves, yet the underlying molecular mechanisms are still largely unresolved (Sun et al., 2022; Xie et al., 2024; Zhang et al., 2024b; Li et al., 2025a).

The Manila clam (*Ruditapes philippinarum*), a widely used sentinel species for marine pollution monitoring (Pintado-Herrera et al., 2020; Qian et al., 2024), was selected as the model organism in this study, with butylated hydroxytoluene (BHT) chosen as a representative SPA (Nieva-Echevarría et al., 2015; Liu and Mabury, 2020; Wang et al., 2024). By integrating transcriptomic analysis, in *silico* prediction, and experimental validation, we systematically characterized the detoxification metabolism of BHT in *R. philippinarum* and elucidated its hepatotoxic effects, with a particular focus on metabolic activation, oxidative stress, and digestive gland injury. These findings provide new insights into the toxicological mechanisms of SPAs in aquatic invertebrates and contribute to a more robust scientific basis for ecological risk assessment of emerging contaminants in marine ecosystems.

2. Materials and methods

2.1. Chemicals and reagents

BHT (2,6-di-tert-butyl-4-methylphenol, ≥ 98 %) was purchased from Beijing Solarbio Science & Technology Co., Ltd (Beijing, China). A certified BHT analytical standard (≥ 99.7 %) was obtained from AccuStandard (New Haven, CT, USA). Analytical standards of the biotransformation products (TPs), including BHT-OH (≥ 99.1 %), BHT-CHO (≥ 99.9 %), BHT-COOH (≥ 99.7 %), and BHT-Q (≥ 98 %), were purchased from TMRM Quality Inspection Technology Co., Ltd (Shanghai, China). The chemical structures and predicted physicochemical properties of the five target compounds are provided in Table S1 and Fig. S1 of the Supporting Information (SI), respectively. Isotopically labeled internal standards, including 2,6-di(tert-butyl-d_9)-4-methylphenol-3,5-O-d_3 (BHT-d_{21}, 98 %) and methyl 4-hydroxybenzoate-2,3,5,6-d_4 (MeP-d_4) were sourced from Toronto Research Chemicals Inc. (Toronto, Canada) and J&K Scientific Ltd. (Beijing, China), respectively. HPLC-grade methanol (MeOH), dichloromethane (DCM), and hexane (Hex) were purchased from Sigma-Aldrich. Ultrapure water (18.2 MΩ·cm) was prepared using Elix® Essential 5 UV Water Purification System (Millipore SAS, Germany).

2.2. Animal study

All animal procedures complied with national guidelines for laboratory animal welfare and were approved by the Institutional Animal Care and Use Committee of Ocean University of China (Qingdao, China). Adult Manila clams (*R. philippinarum*) were collected from the tidal flats of Hongdao (Qingdao, China), with average shell height and length of 2.4 ± 0.3 cm and 3.3 ± 0.2 cm, respectively. Clams were acclimated for 7 days in polyethylene tanks (66 L; 60 cm × 50 cm × 35 cm) containing 40 L of natural seawater collected from the nearshore Qingdao (salinity: 31; pH: 7.6 ± 0.2; temperature: 18 ± 0.5 °C). Aeration was maintained continuously, and 50 %-67 % of the water was renewed daily. Clams were maintained at a density of 12–15 individuals per liter and fed 5 mg/L of *Spirulina* powder daily to stabilize physiological status. Toxicity exposures were conducted in the same tank system, with 500 healthy clams randomly assigned per treatment group. In this study, environmentally relevant BHT exposure concentrations (0, 20, 100, and 200 μg/L) were established based on available monitoring data for marine SPAs (Wang et al., 2018a, 2018b) and our unpublished measurements of 16 SPAs in nearshore waters of the Shandong Peninsula. In addition, the exposure design accounted for the benthic lifestyle of *R. philippinarum* and the substantial exposure burden associated with the strong bioaccumulative potential of SPAs. Preliminary tests confirmed that the water solubility of BHT was < 1 mg/L, consistent with values reported in the EPA PubChem database (0.4–0.6 mg/L; SI Section 1.1). The highest concentration remaining below the solubility limit, ensuring the physicochemical feasibility of the exposure design. BHT stock solution were prepared in dimethyl sulfoxide (DMSO, Sigma), and stored at 4 °C. Each treatment, including the control (containing 0.001 % DMSO, v/v), was conducted in triplicate. Natural seawater (40 L per tank) was replaced daily (100 %) with freshly prepared seawater containing BHT at the designated concentrations. Measured BHT concentrations at the beginning of exposure (0 h) were consistent with the nominal levels, and 24 h concentrations were also measured (Table S2). A 12 h light/12 h dark photoperiod was maintained throughout the 28-day experiment, which consisted of a 21-day exposure phase (days 0–21) and a 7-day depuration phase (days 22–28). Samples were collected at 0, 1, 6, 12, 21, 22, and 28d for bioaccumulation analysis, biochemical assays, gene expression profiling, and histopathological examination. Detailed sampling procedures are provided in the SI Section 1.2.

2.3. Sample preparation and instrumental analysis

Stock solutions of BHT, its TPs, BHT-d_{21}, and MeP-d_4 were prepared in methanol and stored at 4 °C. Working solutions were freshly prepared by diluting the stock solutions prior to each analysis. Poly-Sery HLB Pro SPE cartridges (60 mg/3 mL; SBEQ-CA6679) were purchased from Anpel Laboratory Technologies Co., Ltd. (Shanghai, China). Sample preparation for water and tissue matrices and quantitative of target SPAs were based on previously published methods, with minor modifications (Wang et al., 2018a, 2018b; Du et al., 2019). Detailed protocols are provided in SI Section 1.3. BHT quantification was performed using a Shimadzu GCMS-QP2020 NX gas chromatograph–mass spectrometer (Shimadzu, Japan) operating in selected ion monitoring (SIM) mode. Chromatographic separation was achieved using an SH-Rxi-5Sil MS capillary column (30 m × 0.25 mm i.d., 0.25 μm film thickness). TPs were analyzed using an Agilent 1260 Infinity II liquid chromatography system coupled to an Ultivo TQ triple quadrupole mass spectrometer (LC-MS/MS, Agilent Technologies, USA) equipped with electrospray ionization (ESI) operating in negative multiple reaction monitoring (MRM) mode. Chromatographic separation was performed on an Agilent ZORBAX RRHD Eclipse Plus C18 column (2.1 × 50 mm, 1.8 μm). Instrumental conditions and MRM transitions are detailed in SI Section 1.4 and Table S3. Representative chromatograms are presented in Fig. S3 and Fig. S4.

2.4. Quality assurance and quality control

Each batch of 10 samples included a procedural blank, matrix samples, and matrix-spiked samples. Calibration curves for each analyte were constructed over ten concentration levels (1, 2.5, 5, 10, 25, 50, 100, 250, 500, and 1000 ng/mL), with correlation coefficients (R^2) $\geq$ 0.997. Analyte concentrations were corrected for the recoveries of internal standards (BHT-d_{21} for BHT and MeP-d_4 for TPs). To prevent carryover, pure solvent (methanol) was injected between samples. Matrix spike recoveries ranged from 77 $\pm$ 18 % for BHT, and from 74 $\pm$ 22 % to 83 $\pm$ 12 % for TPs (Table S4). Limits of quantification (LOQs), defined as a signal-to-noise ratio (S/N) of 10 in matrix, were 4.9 ng/g for BHT, 2.2 ng/g for BHT-OH, 2.5 ng/g for BHT-CHO, 1.2 ng/g for BHT-COOH, and 1.6 ng/g for BHT-Q (Table S4). Limits of detection (LODs) are presented in Table S4.

2.5. Transcriptomic analysis

Transcriptional analysis was performed on digestive glands of *R. philippinarum* collected from the 200 μg/L treatment group at 0, 1, 6, and 12d (n = 3 per time point). RNA-seq libraries were prepared and sequenced on the Illumina NovaSeq 6000 platform (Shanghai Majorbio Biopharm Technology Co., Ltd., Shanghai, China). Raw sequencing data were deposited in NCBI BioProject database under accession number PRJNA1085511. Bioinformatics analyses were conducted using the Majorbio Cloud Platform (www.majorbio.com). Detailed sequencing protocols and bioinformatics workflows are provided in SI Section 1.5.

2.6. In silico prediction

In this study, potential protein targets and nuclear receptors interacting with BHT were identified using PDBbind+COMET (https://www.pdbbind-plus.org.cn/comet) and ADMETlab 3.0 (https://admetlab3.scbdd.com/server/evaluationCal), respectively. Binding affinities for phase I CYP450 enzymes were predicted using ADMETlab 3.0, pkCSM (https://biosig.lab.uq.edu.au/pkcsm/prediction), and admetSAR 3.0 (https://lmmd.ecust.edu.cn/admetsar3/predict.php). Phase I and phase II metabolic pathways, including key detoxification enzymes and intermediate metabolites of BHT, were predicted using BioTransformer 3.0 (https://biotransformer.ca/). Predicted protein targets, nuclear receptors, and metabolic enzymes were filtered for relevance to BHT detoxification pathways, yielding 13 candidate proteins. These proteins were aligned with the *R. philippinarum* genome (alignment procedures and results are provided in SI Section 1.6 and Table S5). The aligned proteins, along with detoxification -related genes identified by transcriptomic analysis, were subjected to molecular docking. Molecular docking of BHT and its TPs (ligands) with the selected protein targets was performed using Molegro Virtual Docker 2019.7 (MVD), employing the MolDock scoring function (Thomsen and Christensen, 2006). Three-dimensional binding interactions were visualized using PyMOL v3.1.4. Detailed docking procedures are described in SI Section 1.7. The hepatotoxicity of BHT and its TPs was predicted using two online tools: the Drug-Induced Liver Injury (DILI) Predictor Model (Seal et al., 2024) (http://srijitseal.com/DILI_Predictor/predictor.html) and the VenomPred 2.0 Model (Di Stefano et al., 2024) (https://www.mmvsl.it/wp/venompred2/).

2.7. Quantitative real-time PCR (qPCR)

Detailed protocols for RNA isolation and qPCR are provided in SI Section 1.8. Ten validation genes were selected based on their consistently significant differential expression across all RNA-seq treatment groups. Additional key genes involved in xenobiotic metabolism and inflammation were identified from the RNA-seq data, while other detoxification -related genes were determined through homology-based alignment. Primer sequences for all target and reference genes were designed using Oligo 7 software and are listed in Table S6. Notable nuclear receptors included the aryl hydrocarbon receptor (*AHR*), aryl hydrocarbon receptor nuclear translocator (*ARNT*), heat shock protein 90 A (*HSP90A*), and hormone receptor-like 96 (*HR96*). The xenobiotic-metabolizing enzymes encompassed cytochrome P450 isoforms (*CYP1A1, CYP1A2, CYP1A1*-like, *CYP2B1*-like, *CYP2C23*-like, *CYP2J4*-like, *CYP2U1*-like, *CYP3A4,* and *CYP3A4*-like), alcohol dehydrogenase 1 (*ADH1*), aldehyde dehydrogenase 1 (*ALDH1*), carbonyl reductase 1 (*CBR1*), uridine diphosphate glucuronosyltransferase (*UGT*), glutathione S-transferase isoforms (*GSTA, GSTO1, GSTT1*), and sulfotransferase isoforms (*SULT1A1, SULT1B1, SULT2A1*). Transporter genes included ATP-binding cassette (ABC) subfamilies *ABCB1, ABCC1, ABCC5*, and *ABCG1/ABCG2*. Inflammatory cytokines genes included tumor necrosis factor (*TNF*) and interleukin-16 (*IL16*). Primer amplification efficiencies ranged from 95.8 % to 103.3 %, with correlation coefficients (R^2) between 0.98 and 0.99. Gene expression levels were normalized to two internal reference genes and calculated using the $2^{\hat{}-\Delta\Delta Ct}$ method (Schmittgen and Livak, 2008).

2.8. Biochemical assays

Protein concentration, methoxyresorufin *O*-demethylase (MROD) and ethoxyresorufin *O*-deethylase (EROD), GST, UGT, superoxide dismutase (SOD), catalase (CAT), glutathione peroxidase (GPX), DNA damage (*F* value), lipid peroxidation (LPO) (MDA content), and protein carbonylation (PC) content were measured. Detailed protocols are provided in SI Section 1.9. SULT activity was assessed using an ELISA kit from Shanghai Enzyme-linked Biotechnology Co., Ltd., while reactive oxygen species (ROS), total antioxidant capacity (T-AOC), and hemolymph aspartate aminotransferase (AST) and alanine aminotransferase (ALT) activities were determined using commercial kits from Nanjing Jiancheng Bioengineering Institute.

2.9. Molecular dynamics simulation

Molecular dynamics (MD) simulations were performed to systematically investigate the interaction between BHT and the dipalmitoylphosphatidylcholine (DPPC) bilayer, aiming to elucidate the potential membrane toxicity of BHT. Modeling, simulation, and analysis of BHT–DPPC interactions were conducted using GROMACS v2024.2 (Abraham et al., 2024). The DPPC Electrostatic potential distribution and Deuterium order parameter ($-S_{CD}$) were calculated directly in GROMACS, while bilayer thickness and area per lipid (APL) were determined using the GridMAT-MD method (Allen et al., 2009). Detailed simulation protocols and parameters are described in SI Section 1.10.

2.10. Histopathological observation

Digestive glands of *R. philippinarum* were fixed in 4 % paraformaldehyde (Beyotime Biotechnology, China) for 24 h, then transferred to 70 % ethanol. Samples were dehydrated through graded ethanol and xylene series and embedded in paraffin. Tissue Sections (4–5 μm thick) were prepared using a Leica RM2016 microtome (Leica, Germany) and stained with hematoxylin and eosin (H&E) (Servicebio, China). Histological observation and imaging were performed using a Nikon ECLIPSE Ci-L fluorescence microscope (Nikon, Japan) to assess tissue structure and pathological changes. Detailed staining and sectioning procedures are provided in SI Section 1.11.

2.11. Statistical analysis

All data are presented as mean $\pm$ standard deviation (Mean $\pm$ SD; n = 3). Statistical analysis was performed using SPSS v25.0 (IBM, Chicago, IL, USA). Data normality and homogeneity of variance were assessed by the Shapiro–Wilk and Levene's tests, respectively. One-way analysis of variance (ANOVA) was used to assess differences among

groups. Dunnett's post hoc test was used for comparisons with the control group (*$p < 0.05$, **$p < 0.01$), and Tukey's post hoc test was applied for multiple pairwise comparisons among all groups (significant differences were indicated by letters, $p < 0.05$). Figures were created using the Majorbio Cloud Platform and CnsKnowall Cloud Platform (https://cnsknowall.com), R v4.4.3 with RStudio v2024.12.1, and Origin 2024.

3. Results

3.1. Identifying detoxification key genes via transcriptomic analysis

To identify key genes involved in BHT detoxification in *R. philippinarum*, RNA-seq was conducted across four exposure durations (0, 1, 6, and 12 d). qPCR validation (Fig. S5C) demonstrated a strong positive correlation with RNA-seq results (Pearson's $r = 0.82$, $R^2 = 0.673$, $P = 2.87 \times 10^{-8}$), confirming data reliability. Differential expression analysis (*P*-value < 0.05 and $|\log_2 FC| \geq 1$) identified 2417 DEGs from pairwise comparisons (1 d vs 0 d, 6 d vs 0 d, and 12 d vs 0 d), including 829 upregulated and 1186 downregulated genes. DEG distributions are shown in the volcano plot (Fig. 1A) and Venn diagram (Fig. S5D). Gene Ontology (GO) enrichment analysis (top 20 terms, *P*-value < 0.01; Fig. 1B) revealed significant enrichment in molecular function (MF, 10 terms), biological process (BP, 9 terms), and cellular component (CC, 1 terms) categories. Key GO terms relevant to detoxification, including monooxygenase activity, oxidoreductase activity, catalytic activity, and NADH oxidase (H_2O_2-forming) activity. Kyoto Encyclopedia of Genes and Genomes (KEGG) pathway enrichment analysis (top 20 pathways, *P*-value < 0.01; Fig. 1C) identified five major detoxification-related pathways: drug metabolism – cytochrome P450, metabolism of xenobiotics by cytochrome P450, drug metabolism – other enzymes, glutathione metabolism, and chemical carcinogenesis – DNA adducts. Hierarchical clustering of 42 detoxification-related genes (Fig. S5E) revealed that most genes exhibited an overall trend of moderate upregulation. Protein–protein interaction (PPI) network analysis (Fig. 1D) identified a core regulatory module centered on *AHR, ABCB1, CYP1A1, CYP1A2,* and multiple *GSTs*, which exhibited high degree centrality, indicating pivotal roles in BHT detoxification. Gene set enrichment analysis (GSEA) of three key KEGG pathways (Fig. S6) further revealed time-dependent pathway activation, with cytochrome

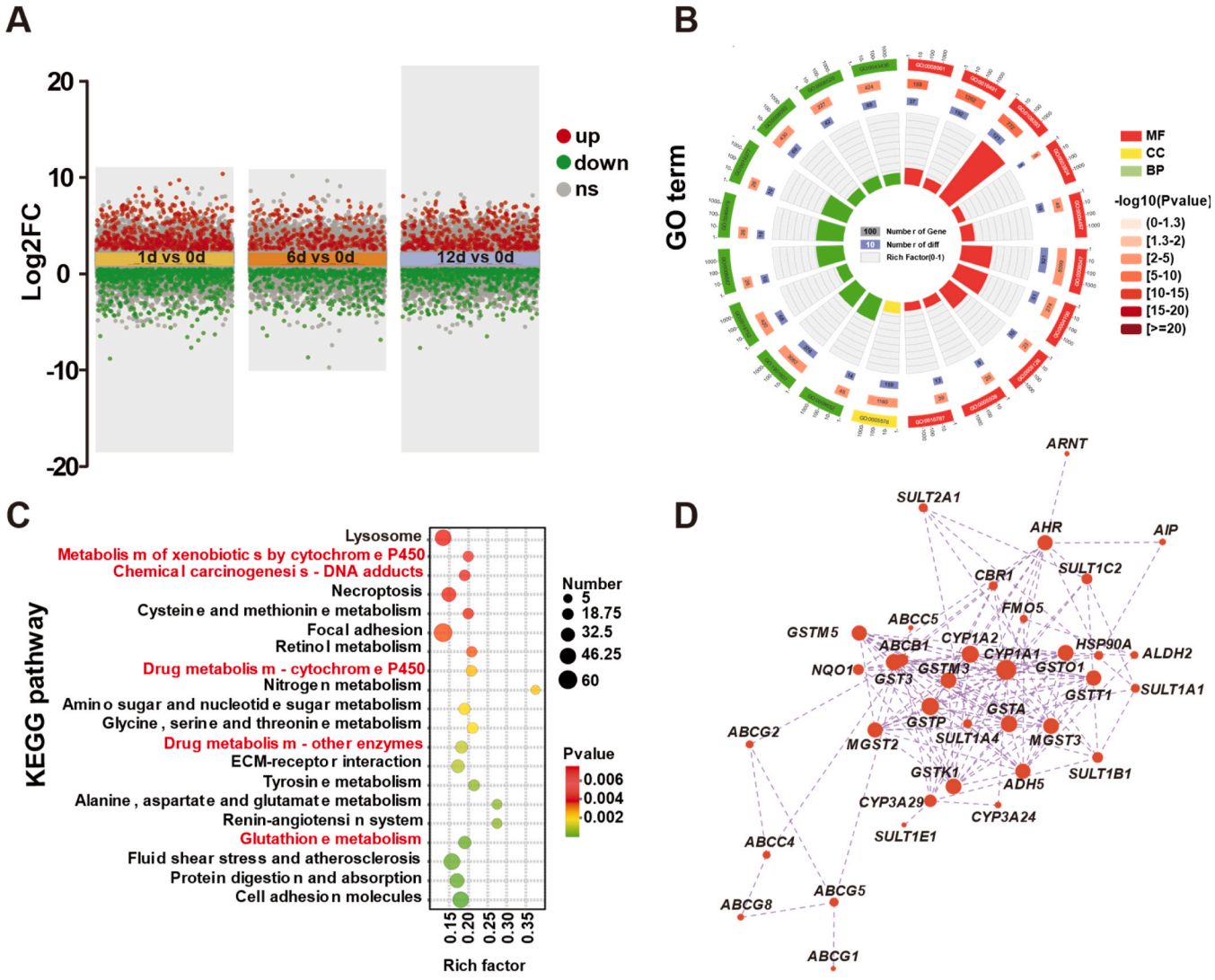

Fig. 1. Transcriptomic analysis of the digestive gland in *Ruditapes philippinarum* under BHT exposure at 0 d, 1 d, 6 d, and 12 d. (A) Volcano plot showing the distribution of significantly upregulated (red) and downregulated (blue) differentially expressed genes (DEGs). (B) Circular plot of Gene Ontology (GO) enrichment across biological process (BP), cellular component (CC), and molecular function (MF) categories. (C) Bubble plot of KEGG pathway enrichment, where bubble size indicates gene counts and color represents significance ($-\log_{10} P$ value). (D) Protein–protein interaction (PPI) network of key detoxification -related genes identified from the transcriptome.

P450-related pathways significantly enriched at 1 d post-exposure (FDR=0.0043, |NES|=1.59; FDR=0.0113, |NES|=1.50) and the "drug metabolism - other enzymes" pathway predominantly enriched at 12 d (FDR=0.0275, |NES|=1.49).

3.2. *In silico prediction of key genes and target proteins involved in BHT detoxification*

In this study, five in *silico* platforms were integrated to predict key genes, protein targets, and metabolic pathways involved in BHT detoxification. COMET-based target prediction (Fig. 2A) identified the nuclear receptor NR1I2 (pregnane X receptor, PXR) as a potential regulatory target (0.19 % matching probability). Tox21 pathway prediction using ADMETlab 3.0 (Fig. 2B) suggested weak binding between BHT and AHR (0–10 %), indicating possible low-affinity signaling involvement. BioTransformer 3.0 simulations (Fig. 2C) predicted six major metabolic reactions, including aliphatic hydroxylation of the methyl group adjacent to the aromatic ring (×1), terminal methyl hydroxylation (×11), aromatic hydroxyl glucuronidation (×9), primary alcohol sulfation (×6), oxidation of primary alcohols to aldehydes (×4), and oxidation of aldehydes to carboxylic acids (×2). These reactions formed a four-tier metabolic network (hydroxylation, oxidation, sulfation, and glucuronidation), generating 32 predicted intermediates and spanning Phase I activation to Phase II conjugation. Phase I metabolism, mediated by CYP450 isoforms (CYP1A2, 2A6, 2B6, 2C8, 2C9, 2C19, 2D6, 2E1, 3A4), exhibited dual reaction modes: (i) aromatic and terminal methyl hydroxylation; (ii) oxidation of primary alcohols to aldehydes and aldehydes to carboxylic acids. Phase II metabolism involved sulfotransferases (SULT, EC 2.8.2.2) and UDP-glucuronosyltransferases (UGT, EC 2.4.1.17), enhancing hydrophilicity and facilitating excretion. Notably, GST-mediated conjugation was not predicted. Substrate/inhibitor analysis of CYP450 isoforms (Table S7) identified CYP1A2, CYP2B6, CYP2C19, and CYP3A4 as key enzymes in BHT metabolism, with CYP3A4 and CYP2B6 showing the highest substrate probabilities.

Molecular docking assessed the binding of BHT and its TPs with 27 detoxification-related proteins in *R. philippinarum* (Tables S8 and S9). Most ligand–protein pairs exhibited favorable affinities, with Moldock scores < –50 kcal/mol, Re-rank scores < –40 kcal/mol, and hydrogen bond energies < –2 kcal/mol. Among these, SULT1A1 showed the strongest binding to BHT, followed by CYP2C23-like and ADH1. CYP1A2 and CYP3A4 also displayed strong interactions, whereas GST family proteins showed weaker binding. Several ABC transporters exhibited relatively high affinities. Hydrogen bond analysis identified key contributions in BHT–CYP1A1 and BHT–ABCC5 interactions, while hydrophobic forces predominated for ADH1, CBR1, and GSTO1. TPs displayed variable affinities across targets (Table S9), with BHT-COOH and BHT-Q showing stronger interactions with CYP450s, SULT1B1, and ABC transporters. Representative 3D docking models (Fig. 2D) illustrated BHT binding to nuclear receptors (AHR, HR96) and key detoxification enzymes (CYP1A1 and UGT), providing structural insights into BHT–protein recognition.

3.3. *Bioaccumulation of BHT/TPs and expression of detoxification genes*

This study systematically characterized BHT detoxification responses, bioaccumulation, and its TPs in *R. philippinarum* using integrated chemical and molecular approaches. qPCR and enzyme activity assays (Fig. 3A) confirmed significant induction ($p < 0.05$) of detoxification-related genes during BHT exposure. Genes associated with the AHR and HR96 pathways were upregulated, together with representative genes from all detoxification phases (Phase 0, I, II, and III). Consistently, enzyme activities of EROD and MROD, as well as UGT, SULT, and GST, were significantly elevated ($p < 0.05$). During depuration (22–28 d), both gene expression and enzyme activities declined, returning largely to baseline by day 28. BHT bioaccumulation in both the digestive gland and soft tissues displayed clear time dependence (Fig. 3B), with continuous uptake during exposure (0–21 d) and substantial elimination during depuration (22–28 d). Concentrations were consistently higher in the digestive gland than in soft tissues. Baseline levels in controls were 9.7 and 7.8 μg/g d.w., respectively, while peak concentrations in the 200 μg/L group reached 31.3 and 21.5 μg/g d.w. on day 21.

Four TPs (BHT-OH, BHT-CHO, BHT-COOH, and BHT-Q) were detected in both tissues (Fig. 3C). BHT-CHO (aldehyde metabolite) was the dominant metabolite (69–84 %), followed by BHT-Q (quinone, 10–27 %), BHT-OH (2–5 %), and BHT-COOH (1–4 %), with aldehyde and quinone metabolites comprising > 90 % of the total TP burden. Metabolite levels increased dose-dependently and showed temporal patterns similar to BHT. Total TP concentrations were approximately twofold higher in the digestive gland (~8000 ng/g d.w.) than in soft tissues (~4000 ng/g d.w.), indicating the digestive gland as the primary site of BHT biotransformation.

3.4. *Hepatotoxicity of BHT*

In silico analysis predicted hepatotoxic potential for BHT and its TPs, mainly linked to hydroxyl group–mediated activation sites (probability >50 %, Fig. S7). Oxidative stress analyses (Fig. 4) showed that BHT exposure significantly increased ROS levels in the digestive gland in a dose-dependent manner ($p < 0.05$; Fig. 4A). After depuration (22–28 d), ROS levels remained elevated in the medium- and high-exposure groups. T-AOC increased during early exposure (0–6 d) but declined markedly during later exposure (12–21 d) ($p < 0.05$). Following depuration, T-AOC remained higher in the 100 and 200 μg/L groups than in controls (Fig. 4B). Activities of antioxidant enzymes (SOD, CAT, and GPX) followed similar patterns, with early induction, subsequent suppression, and sustained elevation in the high-exposure group during depuration ($p < 0.05$, Fig. 4C). Consistent with oxidative imbalance, lipid peroxidation (MDA), protein carbonylation (PC), and DNA damage (*F* value) increased significantly in a dose-dependent manner ($p < 0.05$), with incomplete recovery after depuration (Fig. 4D).

Molecular dynamics simulations further supported BHT-induced membrane toxicity. BHT altered DPPC bilayer thickness distributions and increased area per lipid (APL), indicating membrane expansion and disorder (Figs. 5A and 5B). In the pure DPPC system (100 ns), bilayer thickness ranged from 2.8 to 4.4 nm (mean: 3.77 nm), consistent with theoretical and experimental values. In the BHT-DPPC systems, the thickness distributions were altered to 3.2–4.2 nm at 200 ns (mean: 3.81 nm) and 3.0–4.2 nm at 400 ns (mean: 3.69 nm), following the order: BHT-DPPC (200 ns) > pure DPPC > BHT-DPPC (400 ns). The average APL (Fig. S8) was 63.37 Å^2 in the pure DPPC bilayer, 63.19 Å^2 in the BHT-DPPC system at 200 ns, and increased to 64.81 Å^2 at 400 ns, with the trend: BHT-DPPC (400 ns) > pure DPPC > BHT-DPPC (200 ns). Electrostatic potential was elevated in BHT–DPPC systems relative to pure DPPC, with minimal differences between 200 and 400 ns simulations (Fig. 5C). Deuterium order parameters ($-S_{CD}$) decreased across carbon atoms, in agreement with theoretical predictions, reflecting reduced membrane order following BHT exposure (Fig. 5D). Consistently, qPCR analysis revealed significant induction of pro-inflammatory cytokines (*TNF* and *IL16*) during exposure ($p < 0.05$), with expression largely normalizing after depuration (Fig. 5E). Hemolymph AST and ALT activities were significantly elevated during exposure and remained partially elevated after depuration. Histopathological observation of digestive gland (Fig. S9) revealed typical hepatotoxic lesions under BHT exposure, including disorganized cellular architecture, epithelial discontinuity, luminal dilation, widened interstitial spaces, inflammatory cell infiltration, hemocyte aggregation, cellular swelling and vacuolation, karyorrhexis, and pyknosis. These pathological alterations intensified with increasing exposure concentration and duration.

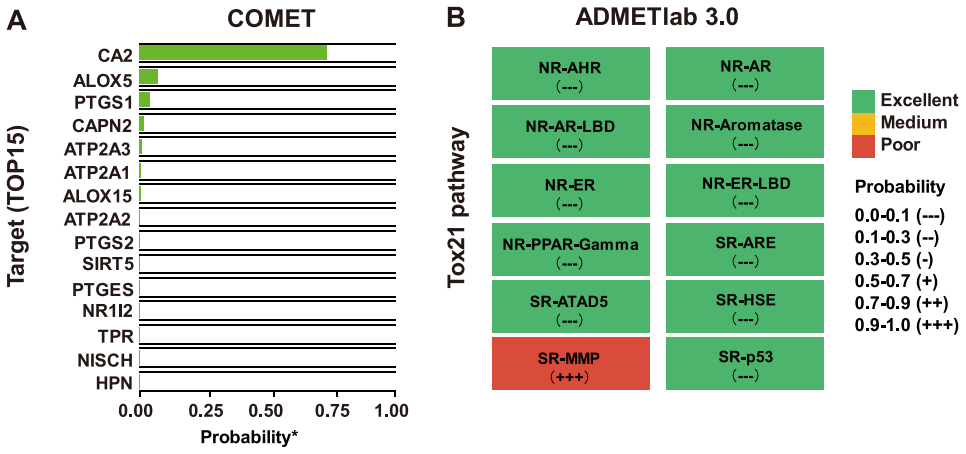

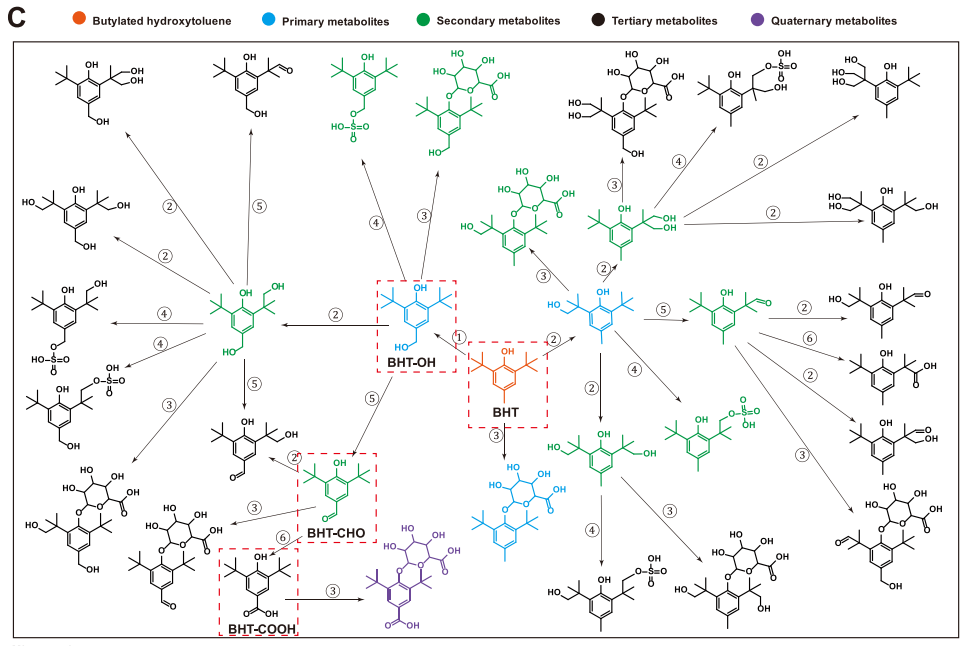

Mian reaction:
① Aliphatic hydroxylation of methyl carbon adjacent to aromatic ring AndFromCyProduct (CYP1A2; CYP2A6; CYP2B6; CYP2C8; CYP2C9; CYP2C19; CYP2D6; CYP2E1; CYP3A4)
② Hydroxylation of terminal methyl (CYP1A2; CYP2A6; CYP2B6; CYP2C8; CYP2C9; CYP2C19; CYP2D6; CYP2E1; CYP3A4)
③ Aromatic OH - glucuronidation (EC 2.4.1.17_UGT)
④ Sulfation of primary alcohol (EC 2.8.2.2_SULT)
⑤ Oxidation of primary alcohol to aldehyde (CYP1A2; CYP2E1; CYP3A4)
⑥ Aldehyde oxidation AndFromCyProduct (CYP1A2; CYP3A4)

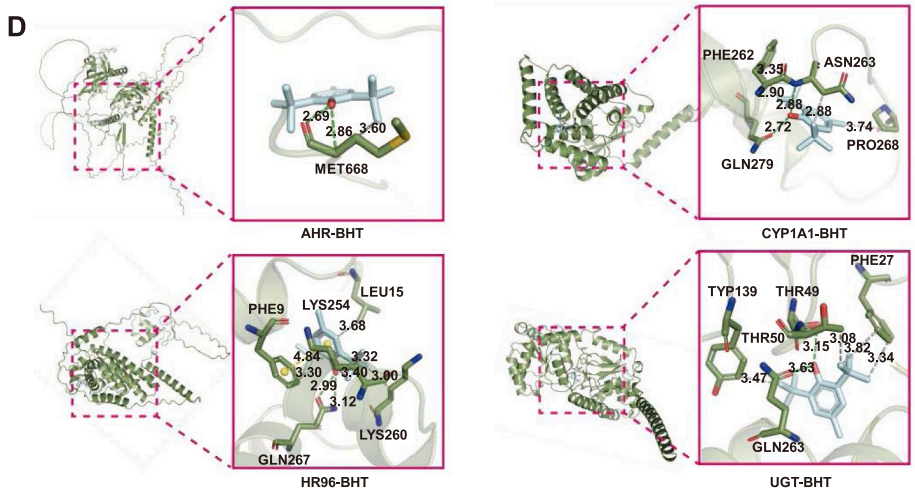

(caption on next page)

Fig. 2. In *silico* prediction of molecular targets and metabolic pathways of BHT. (A) Top 15 predicted protein targets of BHT identified using the PDBbind+COMET platform (https://www.pdbbind-plus.org.cn/comet), ranked by interaction probability. (B) Predicted binding affinities of BHT to nuclear receptors from the ADMETlab 3.0 platform (https://admetlab3.scbdd.com/server/detail/tmpl0t3ax6v1744943841/0), with disruption potential color-coded as green (high), orange (moderate), and red (low). (C) Comprehensive in *silico* prediction of Phase I and Phase II metabolic pathways of BHT using the BioTransformer 3.0 "All Human" model (https://biotransformer.ca/queries/141758/status?query_smiles=), including key enzymes, metabolic routes, and predicted metabolites. (D) Three-dimensional (3D) molecular docking models of BHT with AHR, HR96, CYP1A1, and UGT. Both overall and close-up views of the binding interactions between BHT and each target protein are presented. In the local views, BHT is depicted as pale cyan sticks, and binding site residues are shown as smudge-style cartoons. Green dashed lines indicate hydrogen bonds, gray dashed lines represent hydrophobic interactions, and yellow dashed lines denote π–π stacking interactions.

4. Discussion

Elucidating the detoxification mechanisms of emerging contaminants (ECs) is essential for understanding their toxicological effects. Recent advances in transcriptomics and in *silico* prediction have substantially improved the resolution of xenobiotic metabolic pathways (Lv et al., 2024). In bivalves, the AHR pathway is widely recognized as a central regulator of organic contaminant detoxification, while in mollusks, HR96—a homolog of the vertebrate PXR/CAR nuclear receptor family (NR1J)—has also been implicated in xenobiotic metabolism (Cruzeiro et al., 2016). For instance, BHT has been reported to significantly upregulate AhR subtypes (*AhR2R* and *AhR2β*) in Atlantic salmon (*Salmo salar*), supporting the involvement of the AhR signaling pathway in BHT-induced detoxification responses (Holaas et al., 2008). In this study, integrative analyses identified AHR and HR96 as the central nuclear receptors regulating BHT detoxification in *R. philippinarum*, consistent with their established roles in vertebrates and mollusks. Notably, this study is the first to identify AHR and HR96 as key nuclear transcription factors mediating SPA detoxification in aquatic invertebrates. These receptors orchestrated a canonical multistage detoxification cascade spanning Phases 0–III. Prior studies have demonstrated that BHT significantly induces Phase I enzymes (e.g., CYP2B and CYP3A), and Phase II enzymes (e.g., GST) in rats (Manson, 1997), and upregulates *CYP1A* and *UGT1* genes in Atlantic salmon (*S. salar*) in a dose- and time-dependent manner (Holaas et al., 2008). In addition, non-CYP450 enzymes (e.g., *ADH1*, *ALDH1*, and *CBR1*) in vertebrates have been shown to contribute to Phase I metabolism via redox cascades, acting synergistically with CYP450 enzymes (Fukami et al., 2022). Consistent with these findings, transcriptomic and computational analyses revealed that BHT metabolism in *R. philippinarum* is dominated by Phase I oxidation mediated by CYP450 enzymes—particularly CYP1A1, CYP1A2, CYP3A4, and CYP2B6—followed by Phase II conjugation, with glucuronidation representing the primary conjugation pathway. Non-CYP enzymes (ADH1, ALDH1, and CBR1) also exhibited marked transcriptional responses, indicating their synergistic involvement in BHT biotransformation. All predicted enzymes were experimentally validated, providing robust support for the proposed detoxification network.

Previous studies have identified the major metabolites of BHT in vertebrates as BHT-OH, BHT-CHO, BHT-COOH, and BHT-Q, with the metabolic sequence typically following the pathway: BHT → BHT-OH → BHT-CHO → BHT-COOH → BHT-Q. In this pathway, both BHT-CHO and BHT-COOH are considered potential precursors of BHT-Q (Nieva-Echevarría et al., 2015). In the present study, metabolite profiling of BHT in *R. philippinarum* revealed a distinct distribution pattern. BHT-CHO was the predominant metabolite, accounting for 69 %–84 % of the total metabolites, followed by BHT-Q (10 %–27 %), both substantially exceeding the levels of BHT-OH (2 %–5 %) and BHT-COOH (1 %–4 %). Together, aldehydic and quinone metabolites comprised more than 90 % of the total metabolite pool. The formation of BHT-CHO is facilitated by methyl group oxidation initiated by hydroxyl radicals (•OH), with its lower activation energy favoring accumulation (Wang et al., 2019). BHT-Q, the terminal product of this pathway, contains a stable conjugated quinone ring structure (–C═O). Interestingly, the higher abundance of BHT-CHO relative to the structurally more stable BHT-Q may be attributed to the catalytic activity of carbonyl reductase 1 (CBR1), which reduces BHT-Q to the less toxic BHT-CHO, thereby mitigating its cytotoxic effects on DNA, proteins, and lipids (Nieva-Echevarría et al., 2015; Fukami et al., 2022). Based on these findings, we propose that BHT-CHO and BHT-Q are the principal metabolites of BHT in mollusks, likely resulting from the rapid conversion of intermediate species such as BHT-OH and BHT-COOH into these more stable end products. Tissue-specific differences in the concentrations of BHT and its metabolites were evident, with notably higher accumulation observed in the digestive gland, underscoring its pivotal role as the primary detoxification organ in bivalves (Lobo-da-Cunha, 2019). Notably, BHT exhibited slow accumulation and elimination kinetics, which may be attributed to steric hindrance from its bulky tert-butyl groups. This observation is consistent with previous reports of slow BHT clearance in various species (Holaas et al., 2008; Nieva-Echevarría et al., 2015). It remains unclear whether other SPAs exhibit similar bioaccumulation and elimination kinetics.

A cascade detoxification network of BHT in *R. philippinarum* was proposed (Fig. 6), comprising the following phases: (1) Phase 0—direct efflux of BHT mediated by P-glycoprotein (P-gp) transporters at the cell membrane; (2) cytoplasmic recognition of BHT by the nuclear receptors AHR and HR96, followed by nuclear translocation and heterodimerization with ARNT and RXR, respectively, thereby activating xenobiotic response elements (XRE/XREM) to regulate detoxification-related gene expression; (3) Phase I—hydroxylation of BHT by CYP1A1, CYP1A2, or CYP3A4 to generate BHT-OH, further oxidation to BHT-CHO catalyzed by CYP1A2 or ADH1, and subsequent conversion to BHT-COOH by CYP1A2 or ALDH1. In addition, BHT may be directly oxidized to BHT-Q by CYP3A4, while both BHT-CHO and BHT-COOH can also act as precursors for BHT-Q formation. Furthermore, BHT-Q may undergo reduction back to BHT-CHO via carbonyl reductase 1 (CBR1); (4) Phase II—direct glucuronidation of BHT by UGT and conjugation of Phase I metabolites via UGT, SULT, and GST, enhancing their hydrophilicity; and (5) Phase III—active efflux of conjugated metabolites mediated by ABC transporters, such as ABCC2/ABCC5 and ABCG1/ABCG2.

Beyond detoxification, increasing evidence supports SPAs as hepatotoxicants. For example, BHT has been reported to induce dose- and time-dependent hepatocellular vacuolization and necrosis in rats (Safer and AI-Nughamish, 1999). Similarly, 3-butylated hydroxyanisole (3-BHA) exacerbates hepatic triglyceride accumulation and steatosis in high-fat diet-fed mice by disrupting lipid metabolism-associated gene expression and altering lipid profiles, thereby accelerating the progression of NAFLD (Sun et al., 2022). Exposure to 2,4-di-tert-butylphenol (2,4-DTBP) induces hepatotoxicity in carp (*Cyprinus carpio*), characterized by apoptosis, oxidative stress, autophagy disruption, and activation of PPARs/NF-κB-mediated inflammatory pathways in a dose-dependent manner (Xie et al., 2024). In the present study, in *silico* predictions using DILI models and the VenomPred 2.0 platform further support the hepatotoxic potential of BHT and its TPs, with predicted probabilities exceeding 50 %, primarily mediated by hydroxyl group-associated activation sites (Fig. S7). BHT exposure disrupted antioxidant defense systems in the digestive gland, as reflected by decreased T-AOC and antioxidant enzyme activities and elevated ROS levels. This redox imbalance triggered biomacromolecular damage, including lipid peroxidation and protein carbonylation, likely exacerbated by the accumulation of reactive metabolites such as BHT-CHO and BHT-Q. These findings establish oxidative stress as a central mechanism underlying BHT-induced hepatotoxicity in bivalves.

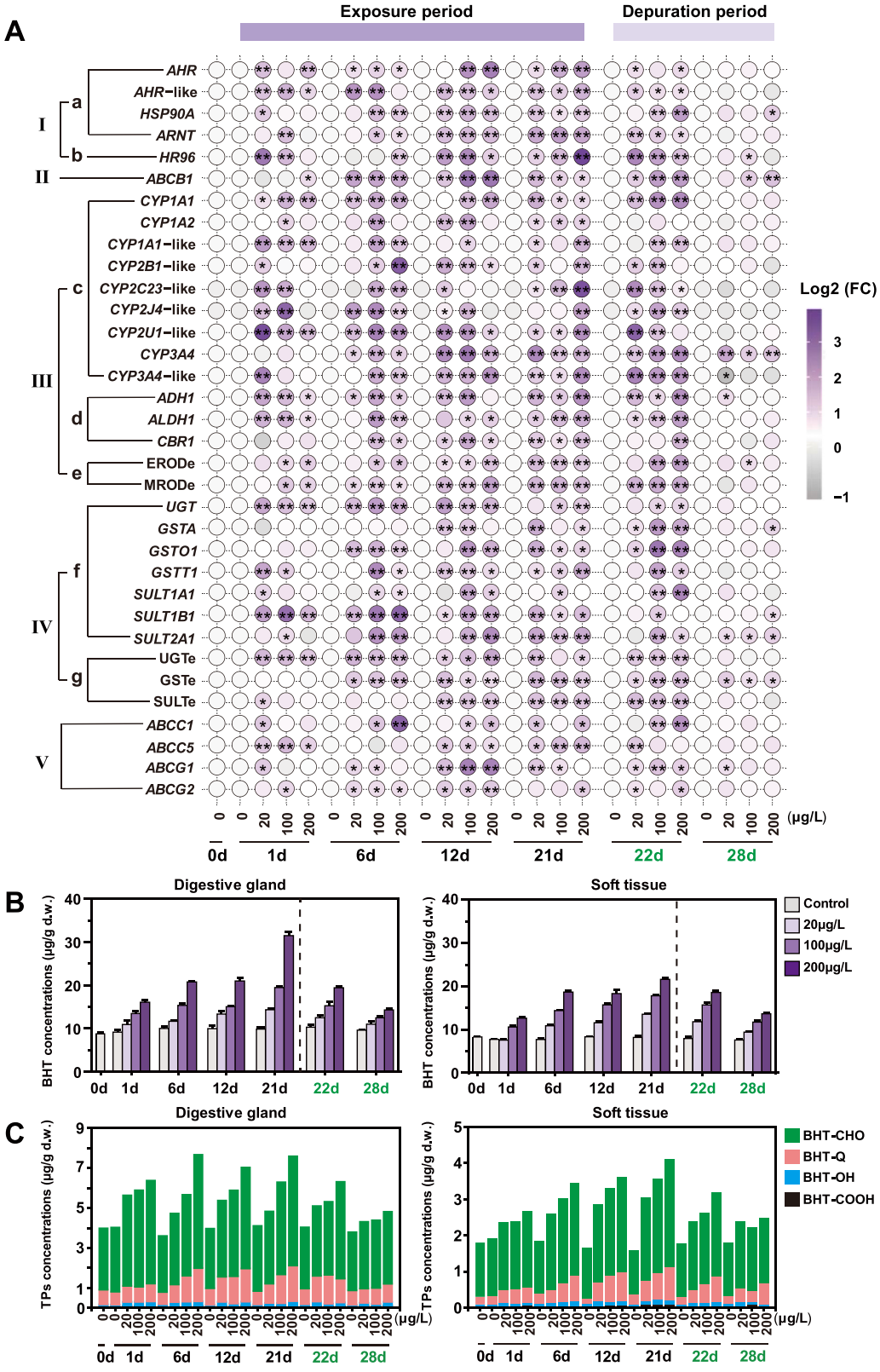

Fig. 3. Detoxification responses in *Ruditapes philippinarum* under BHT exposure. (A) Heatmap of gene expression and enzymatic activity in the digestive gland, highlighting key detoxification pathways: I – Signaling pathways (a: AHR pathway genes; b: HR96 nuclear receptor); II – ABCB1 gene (P-glycoprotein); III – Phase I metabolism (c: CYP family genes; d: other Phase I genes; e: Phase I enzyme activities); IV – Phase II metabolism (f: UGT, GST, and SULT genes; g: Phase II enzyme activities); V – ABC transporter genes. All expression and activity data were normalized as $\log_2$ fold changes ($\log_2$FC). (B) BHT concentrations in the digestive gland and soft tissues. (C) Banded plots showing the relative concentrations of four BHT metabolites (BHT–OH, BHT–CHO, BHT–COOH, and BHT–Q) in the digestive gland and soft tissues. The suffix "e" in terms such as MRODe indicates enzyme activity assays. Data are presented as mean ± SD (n = 3). Asterisks denote significant differences from the control (one-way ANOVA with Dunnett's post hoc test, $^{*}p < 0.05$, $^{**}p < 0.01$).

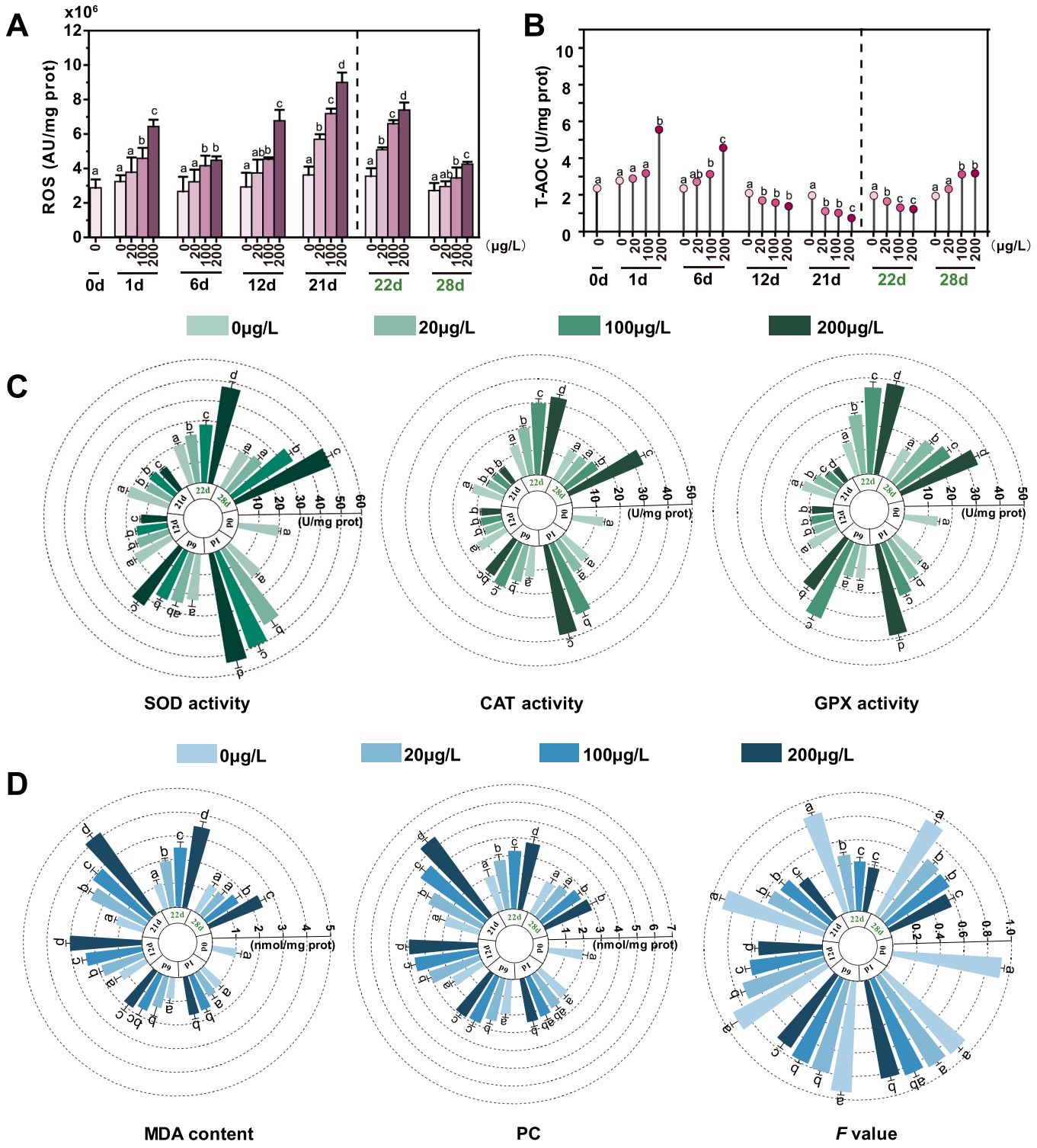

Fig. 4. BHT-induced oxidative stress in the digestive gland of *Ruditapes philippinarum*. (A) ROS levels; (B) T-AOC levels; (C) Activities of SOD, CAT, and GPX; (D) Biomacromolecular damage indicators, including LPO (represented as malondialdehyde [MDA] content), PC, and DNA damage (represented as the *F* value). Data are presented as mean ± SD (n = 3). Different letters indicate statistically significant differences compared to the control group (one-way ANOVA with Tukey's post hoc test, $p < 0.05$).

Inflammation is another hallmark of hepatotoxicity. In carp (*C. carpio*), 2,4-DTBP activates the NF-κB pathway, upregulates inflammatory cytokines (*TNF-α*, *IL-1β*, and *IL-6*), increases serum ALT and AST levels, and induces nuclear condensation, inflammatory cell infiltration, and hepatocyte apoptosis (Xie et al., 2024). Similarly, in the Asian clam (*Corbicula fluminea*), 2,4-DTBP exposure increases IL-1 and NF-κB expression in the digestive gland, indicating a hepatic inflammatory response (Zhang et al., 2024). Molecular dynamics simulations further demonstrated that BHT directly perturbs DPPC bilayer structure, altering membrane thickness, lipid packing, electrostatic potential, and membrane order, thereby compromising membrane integrity. These biophysical disruptions were accompanied by inflammatory responses,

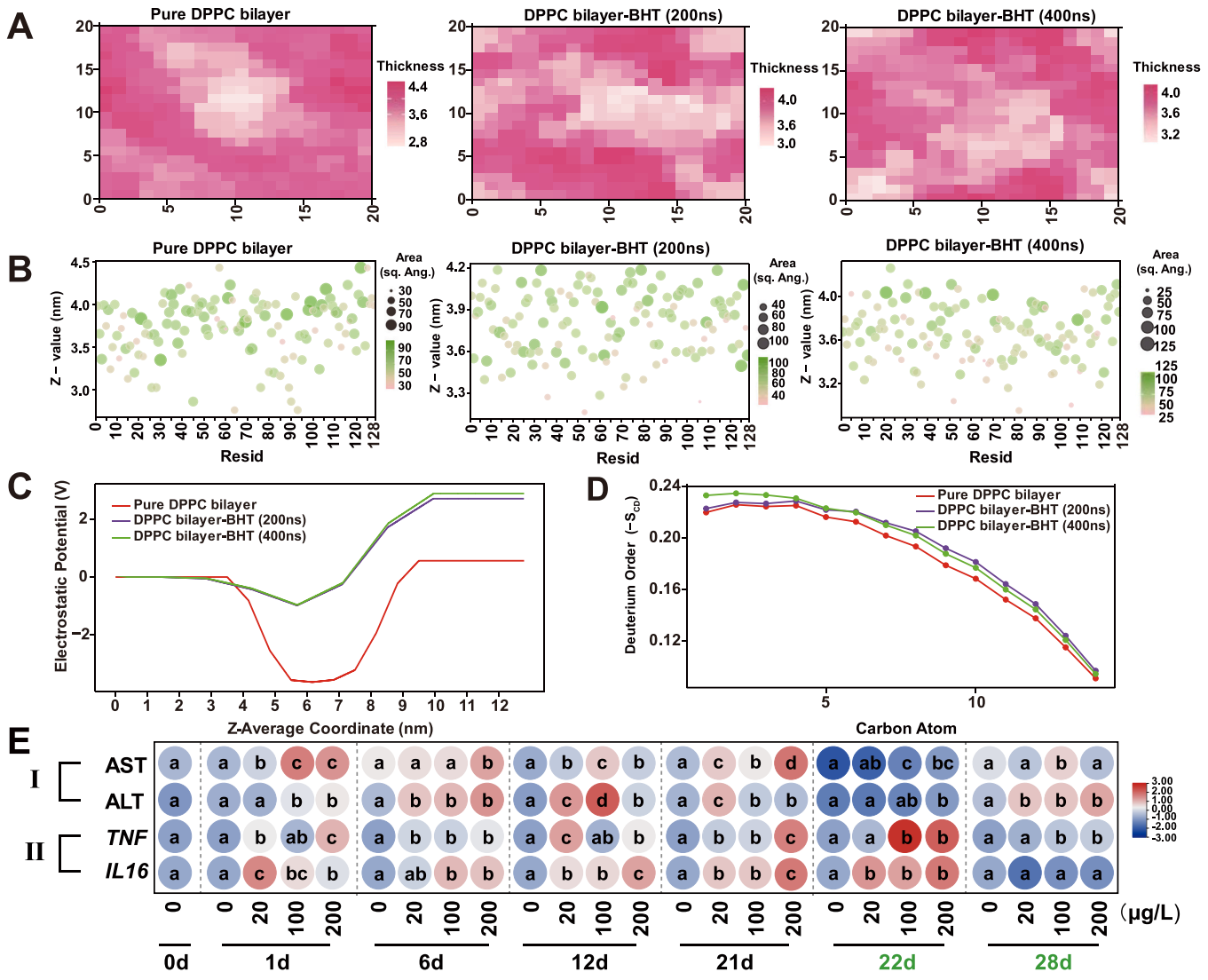

Fig. 5. Molecular dynamics (MD) simulations and histopathological analyses of BHT-induced hepatic (digestive gland) toxicity in *Ruditapes philippinarum*. (A–D) MD simulations of the DPPC bilayer showing changes in (A) bilayer thickness, (B) area per lipid (APL), (C) electrostatic potential distribution, and (D) deuterium order parameter ($-S_{CD}$) of lipid acyl chains following BHT interaction. (E) Heatmap of hemolymph AST and ALT levels and gene expression of pro-inflammatory cytokines *TNF* and *IL16* in the digestive gland. Data are presented as mean ± SD (n = 3). Different letters indicate statistically significant differences compared to the control group (one-way ANOVA with Tukey's post hoc test, $p < 0.05$).

including upregulation of pro-inflammatory cytokines, elevated hemolymph ALT and AST levels, and pronounced histopathological lesions in the digestive gland. Collectively, these results provide converging molecular, cellular, and tissue-level evidence of BHT-induced hepatotoxicity. Given their extensive use, persistence, and bioaccumulation potential, SPAs represent an underrecognized ecological risk. The conserved detoxification and stress-response pathways observed in bivalves suggest that similar hepatotoxic mechanisms may operate in other non-target organisms. Importantly, the mechanistic evidence presented here supports the inclusion of SPAs in environmental monitoring and regulatory frameworks to better address their long-term ecological impacts.

5. Conclusion

This study integrated transcriptomic analysis, *in silico* predictions, and experimental validation to elucidate, for the first time, the detoxification pathways of SPAs in aquatic animals. Furthermore, the hepatotoxicity of BHT in mollusks was comprehensively characterized from three interrelated perspectives: metabolism, oxidative stress, and liver injury. BHT metabolism was transcriptionally regulated by the AHR and HR96 nuclear receptor pathways. Phase I enzymes (CYP1A1, CYP1A2, CYP3A4) and the Phase II enzyme UGT were identified as key players in BHT biotransformation. Metabolite profiling revealed the abundance ranking of BHT metabolites as BHT-CHO > BHT-Q > BHT-OH > BHT-COOH. A cascade detoxification pathway was proposed based on *in silico* predictions and experimental validation. BHT exposure impaired antioxidant defense systems, leading to increased ROS production. Hepatotoxicity was demonstrated by converging evidence from membrane toxicity, oxidative damage, and inflammatory responses. Collectively, this study provides novel insights into the detoxification pathways of ECs and establishes a scientific basis for the ecological risk assessment and mechanistic toxicology of SPAs in aquatic invertebrates.

CRediT authorship contribution statement

Pengfei Li: Methodology, Investigation. **Qiaoqiao Wang:** Methodology, Investigation. **Jingjing Miao:** Resources, Methodology. **Luqing Pan:** Supervision, Resources, Project administration, Funding acquisition, Conceptualization. **Ruicheng Qi:** Writing – review & editing,

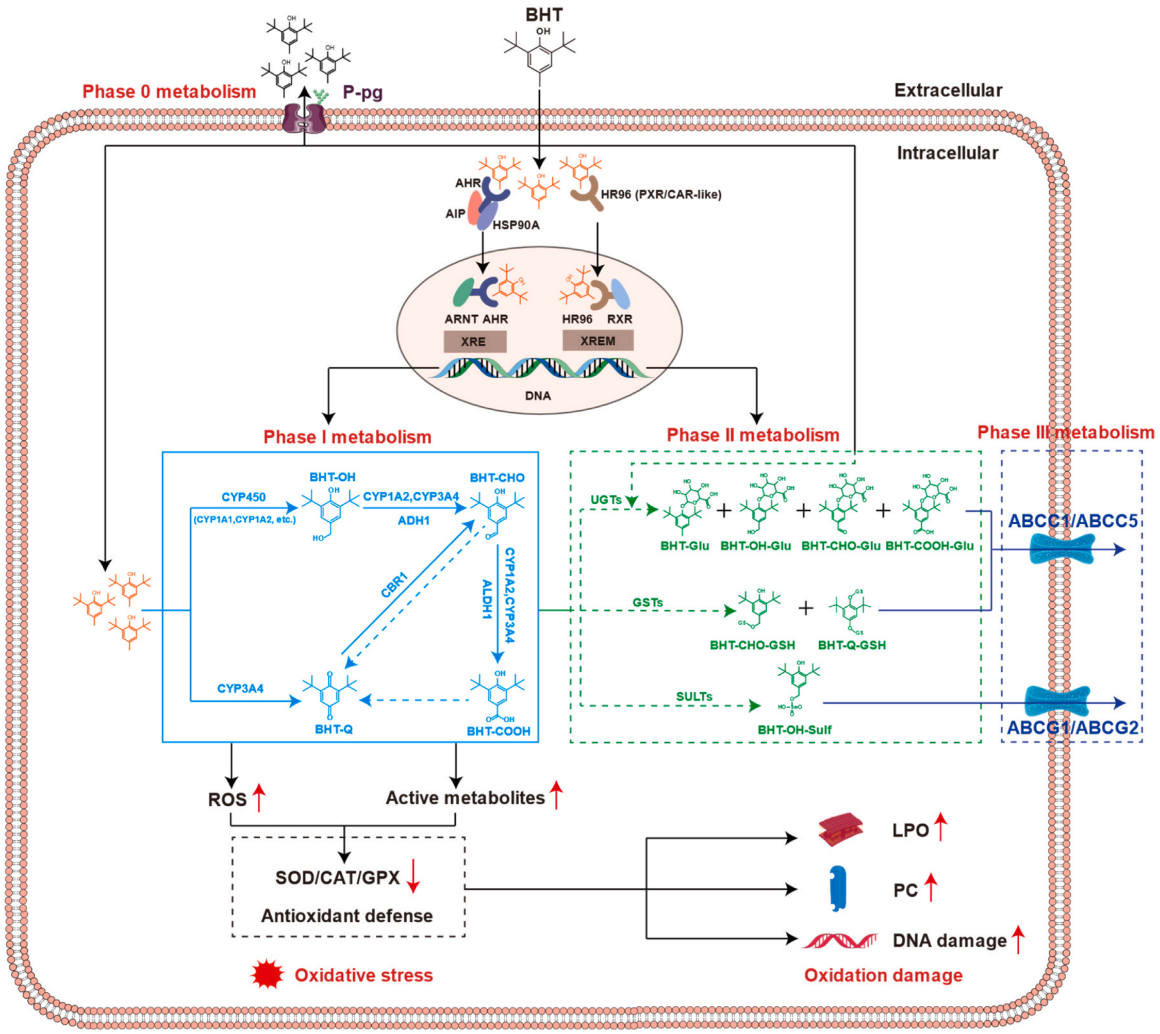

Fig. 6. Illustration of multiphase detoxification and oxidative stress pathways induced by BHT in *Ruditapes philippinarum*.

Writing – original draft, Visualization, Validation, Software, Methodology, Investigation, Formal analysis, Data curation, Conceptualization. **Zeyuan Li:** Writing – review & editing, Supervision, Conceptualization.

Declaration of Generative AI and AI-assisted technologies in the writing process

During the preparation of this work, the authors used ChatGPT (OpenAI) to improve the readability and language of the manuscript. After using this tool, the authors carefully reviewed and edited the content as needed, and we take full responsibility for the content of the published article.

Declaration of Competing Interest

The authors declare that they have no known competing financial interests or personal relationships that could have appeared to influence the work reported in this paper.

Acknowledgments

This work was supported by the National Natural Science Foundation of China (Grant No. 32273106). We gratefully acknowledge the High-Performance Biological Supercomputing Center and the Laboratory of Aquaculture Ecology at Ocean University of China for technical support. We also thank the staff of the Laboratory of Physiology for their assistance with the experiments and Dr. Sobereva for his guidance with molecular dynamics simulations.

Appendix A. Supporting information

Supplementary data associated with this article can be found in the online version at doi:10.1016/j.ecoenv.2026.119677.

Data availability

Data will be made available on request.

References

Abraham, M., Alekseenko, A., Basov, V., Bergh, C., Briand, E., Brown, A., Doijade, M., Fiorin, G., Fleischmann, S., Gorelov, S., Gouaillardet, G., Grey, A., Irrgang, M.E., Jalalypour, F., Jordan, J., Kutzner, C., Lemkul, J.A., Lundborg, M., Merz, P., Miletic, V., Morozov, D., Nabet, J., Pall, S., Pasquadibisceglie, A., Pellegrino, M., Santuz, H., Schulz, R., Shugaeva, T., Shvetsov, A., Villa, A., Wingbermuehle, S., Hess, B., Lindahl, E., 2024. GROMACS 2024.2 Manual. https://doi.org/10.5281/zenodo.11148638.

Allen, W.J., Lemkul, J.A., Bevan, D.R., 2009. GridMAT-MD: a grid-based membrane analysis tool for use with molecular dynamics. J. Comput. Chem. 30, 1952–1958. https://doi.org/10.1002/jcc.21172.

Alofe, O., Kisanga, E., Inayat-Hussain, S.H., Fukumura, M., Garcia-Milian, R., Perera, L., Vasiliou, V., Whirledge, S., 2019. Determining the endocrine disruption potential of industrial chemicals using an integrative approach: public databases, in vitro exposure, and modeling receptor interactions. Environ. Int. 131, 104969. https://doi.org/10.1016/j.envint.2019.104969.

Ashrap, P., Zheng, G., Wan, Y., Li, T., Hu, W., Li, W., Zhang, H., Zhang, Z., Hu, J., 2017. Discovery of a widespread metabolic pathway within and among phenolic xenobiotics. Proc. Natl. Acad. Sci. 114, 6062–6067. https://doi.org/10.1073/pnas.1700558114.

Chai, Y., Sheng, D., Ji, X., Meng, Y., Shen, F., He, R., Ma, R., Wang, Y., 2023. Developmental and neurobehavioral toxicity of 2,2′-methylenebis(6-tert-butyl-4-methylphenol) (antioxidant AO2246) during the early life stage of zebrafish. Sci. Total Environ. 899, 166306. https://doi.org/10.1016/j.scitotenv.2023.166306.

Chibwe, L., Titaley, I.A., Hoh, E., Simonich, S.L.M., 2017. Integrated framework for identifying toxic transformation products in complex environmental mixtures. Environ. Sci. Technol. Lett. 4, 32–43. https://doi.org/10.1021/acs.estlett.6b00455.

Cruzeiro, C., Lopes-Marques, M., Ruivo, R., Rodrigues-Oliveira, N., Santos, M.M., Rocha, M.J., Rocha, E., Castro, L.F.C., 2016. A mollusk VDR/PXR/CAR-like (NR1J) nuclear receptor provides insight into ancient detoxification mechanisms. Aquat. Toxicol. 174, 61–69. https://doi.org/10.1016/j.aquatox.2016.02.007.

Di Stefano, M., Galati, S., Piazza, L., Granchi, C., Mancini, S., Fratini, F., Macchia, M., Poli, G., Tuccinardi, T., 2024. VenomPred 2.0: a novel in silico platform for an extended and human interpretable toxicological profiling of small molecules. J. Chem. Inf. Model 64, 2275–2289. https://doi.org/10.1021/acs.jcim.3c00692.

Dong, C., Zheng, G., Peng, J., Guo, M., Wu, H., Tan, Z., 2024. Integrative inducer intervention and transcriptomic analyses reveal the metabolism of paralytic shellfish toxins in azumapecten farreri. Environ. Sci. Technol. 58, 6519–6531. https://doi.org/10.1021/acs.est.4c00607.

Du, B., Zhang, Y., Lam, J.C.W., Pan, S., Huang, Y., Chen, B., Lan, S., Li, J., Luo, D., Zeng, L., 2019. Prevalence, biotransformation, and maternal transfer of synthetic phenolic antioxidants in pregnant women from South China. Environ. Sci. Technol. 53, 13959–13969. https://doi.org/10.1021/acs.est.9b04709.

Fukami, T., Yokoi, T., Nakajima, M., 2022. Non-P450 drug-metabolizing enzymes: contribution to drug disposition, toxicity, and development. Annu. Rev. Pharmacol. Toxicol. 62, 405–425. https://doi.org/10.1146/annurev-pharmtox-052220-105907.

Holaas, E., Bohne, V.B., Hamre, K., Arukwe, A., 2008. Hepatic retention and toxicological responses during feeding and depuration periods in Atlantic Salmon (Salmo salar) fed graded levels of the synthetic antioxidant, butylated hydroxytoluene. J. Agric. Food Chem. 56, 11540–11549. https://doi.org/10.1021/jf8025524.

Johnson, A.C., Jin, X., Nakada, N., Sumpter, J.P., 2020. Learning from the past and considering the future of chemicals in the environment. Science 367, 384–387. https://doi.org/10.1126/science.aay6637.

Li, Z., Qi, R., Wang, Q., Zheng, X., Li, P., Liao, L., Pan, L., 2025a. Study on the detoxification and toxic effects of clam Ruditapes philippinarum exposed to 2,6-ditert-butyl-4-methylphenol (BHT): oxidative stress, neurotoxicity, respiratory toxicity, and immunotoxicity. Environ. Res. 268, 120839. https://doi.org/10.1016/j.envres.2025.120839.

Li, H., Xia, X., Cheng, S., Zang, J., Wang, Z., Du, M., 2023. Oyster (*Crassostrea gigas*) ferritin relieves lead-induced liver oxidative damage *via* regulating the mitophagy. Int. J. Biol. Macromol. 253, 126965. https://doi.org/10.1016/j.ijbiomac.2023.126965.

Li, B., Xu, C., Zhang, D., Wang, S., Xu, J., Xiao, B., Feng, Y., Fu, H., Chen, X., Zhang, Z., 2025b. Combined analysis of network toxicology and multiomics revealed the potential mechanism of 6PPDQ-induced hepatotoxicity in mice. Environ. Sci. Technol. 59, 10204–10214. https://doi.org/10.1021/acs.est.5c03906.

Li, S., Zhao, M., Zhang, S., Yang, R., Yin, N., Wang, H., Faiola, F., 2024. Assessing developmental neurotoxicity of emerging environmental chemicals using multiple in vitro models: a comparative analysis. Environ. Pollut. 347, 123743. https://doi.org/10.1016/j.envpol.2024.123743.

Liu, R., Mabury, Scott A., 2020. Synthetic phenolic antioxidants: a review of environmental occurrence, fate, human exposure, and toxicity. Environ. Sci. Technol. 54, 11706–11719. https://doi.org/10.1021/acs.est.0c05077.

Liu, W., Zhang, J., Liang, X., Wang, Y., Liu, R., Zhang, R., Zha, J., Martyniuk, C.J., 2022. Environmental concentrations of 2, 4-DTBP cause immunotoxicity in zebrafish (Danio rerio) and may elicit ecological risk to wildlife. Chemosphere 308, 136465. https://doi.org/10.1016/j.chemosphere.2022.136465.

Lobo-da-Cunha, A., 2019. Structure and function of the digestive system in molluscs. Cell Tissue Res 377, 475–503. https://doi.org/10.1007/s00441-019-03085-9.

Lv, M., Liu, Y., Shi, C., Liang, J., Zhao, X., Wang, M., Yan, Y., Gao, J., Yao, L., Liu, J., Fang, M., Liu, R., Qu, G., Cai, Z., Jiang, G., 2024. A missing puzzle piece of pollutant metabolism in humans: The gut microbiota. Environ. Sci. Technol. Lett. 11, 48–50. https://doi.org/10.1021/acs.estlett.3c00833.

Manson, M., 1997. Mechanism of action of dietary chemoprotective agents in rat liver: induction of phase I and II drug metabolizing enzymes and aflatoxin B1 metabolism. Carcinogenesis 18, 1729–1738. https://doi.org/10.1093/carcin/18.9.1729.

Nieva-Echevarría, B., Manzanos, M.J., Goicoechea, E., Guillén, M.D., 2015. 2,6-Di-Tert-Butyl-Hydroxytoluene and Its Metabolites in Foods. Compr. Rev. Food Sci. Food Saf. 14, 67–80. https://doi.org/10.1111/1541-4337.12121.

Petushok, N., Gabryelak, T., Pałecz, D., Zavodnik, L., Szollosi Varga, I., Deér, K.A., 2002. Comparative study of the xenobiotic metabolising system in the digestive gland of the bivalve molluscs in different aquatic ecosystems and in aquaria experiments. Aquat. Toxicol. 61, 65–72. https://doi.org/10.1016/S0166-445X(02)00030-9.

Pintado-Herrera, M.G., Allan, I.J., González-Mazo, E., Lara-Martín, P.A., 2020. Passive Samplers vs Sentinel Organisms: One-Year Monitoring of Priority and Emerging Contaminants in Coastal Waters. Environ. Sci. Technol. 54, 6693–6702. https://doi.org/10.1021/acs.est.0c00522.

Qian, J., Hu, T., Xiong, H., Cao, X., Liu, F., Gosnell, K.J., Xie, M., Chen, R., Tan, Q.-G., 2024. Turbid waters and clearer standards: refining water quality criteria for coastal environments by encompassing metal bioavailability from suspended particles. Environ. Sci. Technol. 58, 5244–5254. https://doi.org/10.1021/acs.est.3c09599.

ReportLinker, 2023. Global synthetic antioxidants market to reach $4 billion by 2030 [WWW Document]. URL ⟨https://www.globenewswire.com/en/news-release/2023/05/05/2662493/0/en/Global-Synthetic-Antioxidants-Market-to-Reach-4-Billion-by-2030.html⟩ (accessed 6.3.25).

Rodrigo, A.P., Costa, P.M., 2017. The role of the cephalopod digestive gland in the storage and detoxification of marine pollutants. Front. Physiol. 8. https://doi.org/10.3389/fphys.2017.00232.

Ruan, T., Li, P., Wang, H., Li, T., Jiang, G., 2023. Identification and Prioritization of Environmental Organic Pollutants: From an Analytical and Toxicological Perspective. Chem. Rev. 123, 10584–10640. https://doi.org/10.1021/acs.chemrev.3c00056.

Safer, A.M., AI-Nughamish, A.J., 1999. Hepatotoxicity induced by the anti-oxidant food additive, butylated hydroxytoluene (BHT), in rats: An electron microscopical study. Histol. Histopathol. 391–406. https://doi.org/10.14670/HH-14.391.

Schmittgen, T.D., Livak, K.J., 2008. Analyzing real-time PCR data by the comparative CT method. Nat. Protoc. 3, 1101–1108. https://doi.org/10.1038/nprot.2008.73.

Seal, S., Williams, D., Hosseini-Gerami, L., Mahale, M., Carpenter, A.E., Spjuth, O., Bender, A., 2024. Improved detection of drug-induced liver injury by integrating predicted in vivo and in vitro data. Chem. Res. Toxicol. https://doi.org/10.1021/acs.chemrestox.4c00015.

Sun, Z., Tang, Z., Yang, X., Liu, Q.S., Zhang, J., Zhou, Q., Jiang, G., 2022. 3- *tert* -Butyl-4-hydroxyanisole Impairs Hepatic Lipid Metabolism in Male Mice Fed with a High-Fat Diet. Environ. Sci. Technol. 56, 3204–3213. https://doi.org/10.1021/acs.est.1c07182.

Thomsen, R., Christensen, M.H., 2006. MolDock: A new technique for high-accuracy molecular docking. J. Med. Chem. 49, 3315–3321. https://doi.org/10.1021/jm051197e.

Tian, D., Yu, Yihan, Yu, Yingying, Lu, L., Tong, D., Zhang, W., Zhang, X., Shi, W., Liu, G., 2023. Tris(2-chloroethyl) phosphate exerts hepatotoxic impacts on zebrafish by disrupting hypothalamic–pituitary–thyroid and gut–liver axes. Environ. Sci. Technol. 57, 9043–9054. https://doi.org/10.1021/acs.est.3c01631.

Wang, Y., He, L., Lv, G., Liu, W., Liu, J., Ma, X., Sun, X., 2019. Distribution, transformation and toxicity evaluation of 2,6-Di-tert-butyl-hydroxytotulene in aquatic environment. Environ. Pollut. 255, 113330. https://doi.org/10.1016/j.envpol.2019.113330.

Wang, X., Hou, X., Hu, Y., Zhou, Q., Liao, C., Jiang, G., 2018a. Synthetic phenolic antioxidants and their metabolites in mollusks from the chinese bohai sea: occurrence, temporal trend, and human exposure. Environ. Sci. Technol. 52, 10124–10133. https://doi.org/10.1021/acs.est.8b03322.

Wang, X., Hou, X., Zhou, Q., Liao, C., Jiang, G., 2018b. Synthetic phenolic antioxidants and their metabolites in sediments from the coastal area of Northern China: spatial and vertical distributions. Environ. Sci. Technol. 52, 13690–13697. https://doi.org/10.1021/acs.est.8b04448.

Wang, F., Xiang, L., Sze-Yin Leung, K., Elsner, M., Zhang, Y., Guo, Y., Pan, B., Sun, H., An, T., Ying, G., Brooks, B.W., Hou, D., Helbling, D.E., Sun, J., Qiu, H., Vogel, T.M., Zhang, Wei, Gao, Yanzheng, Simpson, M.J., Luo, Yi, Chang, S.X., Su, G., Wong, B.M., Fu, T.-M., Zhu, D., Jobst, K.J., Ge, C., Coulon, F., Harindintwali, J.D., Zeng, X., Wang, H., Fu, Y., Wei, Z., Lohmann, R., Chen, C., Song, Y., Sanchez-Cid, C., Wang, Y., El-Naggar, A., Yao, Y., Huang, Y., Cheuk-Fung Law, J., Gu, Chenggang, Shen, H., Gao, Yanpeng, Qin, C., Li, Hao, Zhang, Tong, Corcoll, N., Liu, M., Alessi, D.S., Li, Hui, Brandt, K.K., Pico, Y., Gu, Cheng, Guo, J., Su, J., Corvini, P., Ye, M., Rocha-Santos, T., He, H., Yang, Y., Tong, M., Zhang, Weina, Suanon, F., Brahushi, F., Wang, Z., Hashsham, S.A., Virta, M., Yuan, Q., Jiang, G., Tremblay, L.A., Bu, Q., Wu, J., Peijnenburg, W., Topp, E., Cao, X., Jiang, X., Zheng, M., Zhang, Taolin, Luo, Yongming, Zhu, L., Li, X., Barceló, D., Chen, J., Xing, B., Amelung, W., Cai, Z., Naidu, R., Shen, Q., Pawliszyn, J., Zhu, Y., Schaeffer, A., Rillig, M.C., Wu, F., Yu, G., Tiedje, J.M., 2024. Emerging contaminants: a one health perspective. Innovation 5, 100612. https://doi.org/10.1016/j.xinn.2024.100612.

Wang, Y., Zhao, J., Xu, Y., Tao, C., Tong, J., Luo, Y., Chen, Y., Liu, X., Xu, T., 2023. Uncovering SOD3 and GPX4 as new targets of benzo[α]pyrene-induced hepatotoxicity through metabolomics and chemical proteomics. Redox Biol. 67, 102930. https://doi.org/10.1016/j.redox.2023.102930.

Xie, R., Xu, Y., Ma, M., Wang, X., Zhang, L., Wang, Z., 2023. First metabolic profiling of 4-n-nonylphenol in human liver microsomes by integrated approaches to testing and assessment: metabolites, pathways, and biological effects. J. Hazard. Mater. 447, 130830. https://doi.org/10.1016/j.jhazmat.2023.130830.

Xie, J., Yin, Y., Lin, B., Li, X., Li, Q., Tang, X., Pan, L., Xiong, X., 2024. Autophagy and PPARs/NF-κB-associated inflammation are involved in hepatotoxicity induced by the synthetic phenolic antioxidant 2,4-di-tert-butylphenol in common carp (Cyprinus carpio). Ecotoxicol. Environ. Saf. 284, 116937. https://doi.org/10.1016/j.ecoenv.2024.116937.

Yang, P., Xie, J., Huang, S., Li, X., Deng, L., Zhang, J., Chen, L., Wu, N., Huang, G., Zhou, C., Xiao, L., Shen, X., 2023. Cocktail" of environmental chemicals and early reproductive outcomes of IVF: the insight from paternal and maternal exposure. J. Environ. Manag. 348, 119462. https://doi.org/10.1016/j.jenvman.2023.119462.

Zhang, Y.Y., Huang, J., Liu, YueHong, Zhang, J., Huang, Z., Liu, YouSheng, Zhao, J., Ying, G., 2024a. In vitro metabolism of the emerging contaminant 6PPD-quinone in human and rat liver microsomes: kinetics, pathways, and mechanism. Environ. Pollut. 345, 123514. https://doi.org/10.1016/j.envpol.2024.123514.

Zhang, R., Li, J., Cui, X., 2020. Tissue distribution, excretion, and metabolism of 2,6-di-tert-butyl-hydroxytoluene in mice. Sci. Total Environ. 739, 139862. https://doi.org/10.1016/j.scitotenv.2020.139862.

Zhang, C., Li, X., Flor, S., Ruiz, P., Kruve, A., Ludewig, G., Lehmler, H.-J., 2022. Metabolism of 3-chlorobiphenyl (PCB 2) in a human-relevant cell line: evidence of

dechlorinated metabolites. Environ. Sci. Technol. 56, 12460–12472. https://doi.org/10.1021/acs.est.2c03687.

Zhang, J., Liang, X., Chen, H., Guo, W., Martyniuk, C.J., 2024b. Exposure to environmental levels of 2,4-di-tert-butylphenol affects digestive glands and induces inflammation in Asian Clam (Corbicula fluminea). Sci. Total Environ. 915, 170054. https://doi.org/10.1016/j.scitotenv.2024.170054.

Zhang, Z., Yuan, S., Yang, Z., Liu, Y., Liu, S., Chen, L., Wu, B., 2025. Hepatotoxicity of three common liquid crystal monomers in Mus musculus: differentiation of actions across different receptors and pathways. Environ. Sci. Technol. 59, 1519–1529. https://doi.org/10.1021/acs.est.4c08945.